

PCCP

Accepted Manuscript



This is an *Accepted Manuscript*, which has been through the Royal Society of Chemistry peer review process and has been accepted for publication.

Accepted Manuscripts are published online shortly after acceptance, before technical editing, formatting and proof reading. Using this free service, authors can make their results available to the community, in citable form, before we publish the edited article. We will replace this *Accepted Manuscript* with the edited and formatted *Advance Article* as soon as it is available.

You can find more information about *Accepted Manuscripts* in the [Information for Authors](#).

Please note that technical editing may introduce minor changes to the text and/or graphics, which may alter content. The journal's standard [Terms & Conditions](#) and the [Ethical guidelines](#) still apply. In no event shall the Royal Society of Chemistry be held responsible for any errors or omissions in this *Accepted Manuscript* or any consequences arising from the use of any information it contains.

Poly(3-hydroxybutyrate-co-4-hydroxybutyrate) based nanocomposites: influence of the microstructure on the barrier properties.

Cite this: DOI: 10.1039/x0xx00000x

R. Crétois,^{a,b,c} N. Follain,^{a,b,c} E. Dargent,^{a,d} J. Soulestin,^{e,f} S. Bourbigot,^{f,g} S. Marais,^{a,b,c} and L. Lebrun^{a,b,c*}

Received 00th January 2012,
Accepted 00th January 2012

DOI: 10.1039/x0xx00000x

www.rsc.org/

Poly(3-hydroxybutyrate-co-4-hydroxybutyrate) (P3HB-co-4HB) films containing various contents of organo-modified montmorillonite C30B nanoclay were prepared by melt intercalation. Wide angle X-ray diffraction measurements and transmission electronic microscopy observations evidenced aggregated and intercalated structures with individual nanoclay platelets in the nanocomposites and an orientation of nanoclay. Differential scanning calorimetry measurements showed that the nanoclay did not influence the crystalline structure of the matrix because mainly located in the polymer amorphous phase. The influence of the filler on the barrier properties of the film was evaluated by water diffusion, gas permeation (CO₂, N₂, O₂) and liquid water sorption measurements. A decrease of the N₂ permeability was measured due to the tortuosity effect of the filler associated with a decrease of the solubility within the matrix. The influence of the filler was more marked for O₂ due to the larger decrease of O₂ solubility. In contrast, the CO₂ permeability increased whatever the filler content because of a facilitated transport mechanism due induced by the presence of quaternary ammonium cations on the C30B surface. The decrease of the water permeability with the filler was explained by a competition between the kinetic (diffusivity) and thermodynamic (solubility) contributions defining the permeability process.

1 Introduction

Natural polyester polyhydroxyalkanoates (PHAs) produced by bacteria have recently received a considerable attention due to their good biodegradability and biocompatibility properties^{1,2}. More than one hundred different biopolyesters can be produced with different structures and properties as a function of the bacteria and substrates available^{1,3}. The potential applications of these polymers are medical devices (suture threads, surgical implants, heart valves...) and short time-life materials for food packaging^{4,5}. The most studied PHAs are the homopolymer poly(3-hydroxybutyrate) (P3HB or PHB) and the copolymer poly(3-hydroxybutyrate-co-3-hydroxyvalerate) (P3HB-co-3HV or PHBV) which differ from PHB by the presence of 3-hydroxyvalerate units (3HV). These both thermoplastic polymers exhibit a high crystallinity degree (generally between 50-70 %), a low hydrophilic character^{2,6} and good barrier properties compared to other biopolyesters such as poly(lactic acid) (PLA) and poly(ϵ -caprolactone)^{7,8}. Nevertheless, these polymers are brittle and present a melting temperature close to the degradation temperature which restricts their industrial applications.

The used of the poly(3-hydroxybutyrate-co-4-hydroxybutyrate) (P3HB-co-4HB or P3HB4HB) is an alternative to the PHB or PHBV. This PHA, now produced at a large scale, is a statistical copolymer with physical properties strongly dependent on the

amount of 4-hydroxybutyrate units (4HB). At low 4HB units content, P3HB4HB is semi-crystalline whereas at high 4HB units content it can be considered as an amorphous rubber^{9,10,11}. The presence of 4HB units usually improves the processability and the elongation at break^{12,13}. However, the 4HB units inhibit the crystallisation so that the decrease of the crystallinity degree^{13,14} reduces barrier properties of P3HB4HB compared to PHB and PHBV^{7,15}.

In order to improve the barrier properties of P3HB4HB matrix, the incorporation of layered nanofillers, like montmorillonite, is a relevant solution as suggested in the literature for polymer matrices^{4,16}. Indeed, the addition of an impermeable phase such as nanoclay is supposed to decrease the permeability by increasing the tortuosity due to the increase of the diffusion pathway of penetrating molecules^{17,18}. The key parameters to obtain an effective tortuosity effect are usually a high aspect ratio and a good dispersion and individualisation of the nanoclay platelets in the matrix. The nanoclays are generally organomodified by the addition of a surfactant in order to increase the organophilic character and consequently to improve the affinity between the matrix and the nanoclays^{19,20}. The aim of this work is to study the influence of the incorporation of nanoclays in P3HB4HB matrix on the microstructure and the consequences on its barrier properties. The dispersion quality of the fillers in the matrix would be analysed from the relationship between the structural characterisation and the permeation properties of the

nanocomposites. Different diffusing species (N_2 , O_2 , CO_2 , H_2O) are used in this study to act as molecular probes since able to interact or not with the components of the nanocomposites.

2 Experimental

2.1. Materials

P3HB4HB was supplied by Tianjin Green Bioscience Company (China). The 4HB units content determined by 1H NMR in $CDCl_3$ is 13 mol%. The weight-average molecular weight was estimated at $3.1 \times 10^5 \text{ g.mol}^{-1}$ by gel permeation chromatography. The organomodified nanoclay Montmorillonite was purchased from Southern Clay Products (Rockwood additives, U.S.A.) under the trade name Cloisite[®] 30B (referenced as C30B). The nanoclay surfactant is composed of a long alkyl chain containing one quaternary ammonium cation and two hydroxyl groups (~65% C18, ~30% C16, ~5% C14).

2.2. Preparation of P3HB4HB/C30B nanocomposite films

P3HB4HB matrix and nanoclay were first dried 12 h at 80 °C to remove all residual moisture. Then, they were blended in different proportions (98.5/2.5, 95/5, 92.5/7.5 and 90/10 wt/wt) using a twin-screw extruder (mini Lab II, Haake, Germany) at 160 °C with 50 rpm screw rotation speed. After granulation into pellets, the exact C30B content was determined by thermogravimetric measurements (TGA7, Perkin-Elmer, U.S.A.). Then nanocomposite films were processed by compression moulding (thickness of 200 μm) using a hot press (Scamex, France) according to the cycle: 10 min at 150 °C then 5 min at 150 °C under 120 bar. Finally, the nanocomposite films were cooled at room temperature without pressure. The same thermal process was applied to the P3HB4HB film used as the reference. All nanocomposite films were stored under vacuum in presence of a desiccant (P_2O_5) for 10 days before the experiments.

2.3. Characterisation

2.3.1. Wide angle X-ray diffraction

Wide angle X-ray diffraction (WAXD) measurements were performed on nanocomposite films with a Bragg-Brentano diffractometer (Bruker AXS D8 Advance, Germany) using $CoK\alpha$ radiation source ($\lambda = 1.789 \text{ \AA}$) powered by 40 mA current and 35 kV voltage. The data were acquired on $2\theta = 2^\circ$ - 10° range with a scanning rate of $0.04^\circ \text{ s}^{-1}$.

2.3.2. Transmission Electronic Microscopy

Transmission Electronic Microscopy (TEM) observations were performed using a Tecnai G² 20 (FEI, U.S.A) microscope powered at 200 kV. Before observation, the samples were coated with resin and cut with an ultra-microtome to obtain thickness samples of about 70 nm. From the TEM images a mean aspect ratio α_{exp} was determined by statistical analysis. The value was calculated from the measurement (length and thickness) of all discernable objects on images. The determination of the size was realised using the free software ImageJ (developed by the National Institutes of Health) on at least 60 objects per image.

2.3.3. Differential Scanning Calorimetry

Differential Scanning Calorimetry (DSC) measurements were performed with a DSC 2920 from Thermal Analysis Instruments (U.S.A.). After a calibration step with indium standard ($T_m = 156.6 \text{ }^\circ\text{C}$, $\Delta H_m = 28.66 \text{ J.g}^{-1}$), the following

thermal program was applied on each film sample (8-10 mg): heating from $-40 \text{ }^\circ\text{C}$ to $180 \text{ }^\circ\text{C}$ at $10 \text{ }^\circ\text{C.min}^{-1}$, then 1 min at $180 \text{ }^\circ\text{C}$ followed by a cooling step from $180 \text{ }^\circ\text{C}$ to $20 \text{ }^\circ\text{C}$ at $10 \text{ }^\circ\text{C.min}^{-1}$. The crystallinity degree X_c of the material was calculated from the endothermic peaks obtained during the heating.

$$X_c = \frac{\Delta H_m}{\Delta H_m^0(1 - \phi_w)} \times 100 \quad (1)$$

$\Delta H_m \text{ (J.g}^{-1}\text{)}$ is the melting enthalpy of the sample calculated from the endothermic peak; ΔH_m^0 is the theoretical melting enthalpy of the polymer assumed to be 100 % crystalline (146 J.g^{-1} for PHBV²¹); ϕ_w is the nanoclay mass fraction.

2.3.4. Gas permeation (N_2 , O_2 , CO_2)

Nitrogen, oxygen and carbon dioxide permeation measurements were carried out at 25 °C by using a barometric method based on the time-lag determination²². The measurements were performed by applying 3 bar of gas (Air Liquide, France) to the upstream side of the film sample. The quantity of transferred gas Q through the tested film was monitored until the increase of pressure in downstream side reached a constant value indicating that the stationary state of the permeation process was reached. The permeability coefficient P was calculated from the slope of the experimental curve (dQ/dt):

$$P = \frac{L}{\Delta p} \frac{dQ}{Adt} \quad (2)$$

P is expressed in Barrer unit (1 Barrer = $10^{-10} \text{ cm}^3 \text{ (STP).cm.cm}^{-2}\text{.s}^{-1}\text{.cmHg}^{-1}$); L is the thickness of the film; A is the surface exposed to the diffusion (11.34 cm^2 for N_2 and CO_2 , 5 cm^2 for O_2); Δp is the difference in pressure between the two sides of the film. A time-lag diffusion coefficient D , was calculated from the time-lag, t_L , given by the extrapolation of the steady-state asymptote to the time axis:

$$D = \frac{L^2}{6t_L} \quad (3)$$

The solubility coefficient S was deduced from the ratio of the permeability to diffusion coefficients. The measurements were averaged from at least two experiments per film.

From the gas permeability values, a selectivity coefficient $\alpha_{A/B}$ between two gases A and B was calculated. It is defined as the ratio of the permeability coefficients of the more permeable gas P_A to the less permeable P_B :

$$\alpha_{A/B} = P_A / P_B \quad (4)$$

2.3.5. Water permeation

The water permeation measurements were performed in thermostated chamber (25 °C) using a home-built permeation cell²³ equipped with a chilled mirror hygrometer (General Eastern Instruments, U.S.A.) as detector. Firstly, the film to test ($A = 5 \text{ cm}^2$) was placed between the two compartments of the permeation cell that were dried with a nitrogen gas flow (99.999% of purity, Air Liquide). Then, pure liquid water (MilliQ system, resistivity $18 \text{ } \Omega\text{.cm}^{-1}$) was introduced in the upstream compartment. The water flux J as a function of time t resulting from the water transfer through the film, was recorded in the downstream compartment. At steady state ($J = J_{st}$), the permeability coefficient P (expressed in Barrer unit) was calculated from:

$$P = \frac{J_{st} \times L}{\Delta a_w} \quad (5)$$

Δa_w is the difference in water activity across the film considered as equal to 1 in this work. The reproducibility of water permeation measurements was checked from at least four specimens per film.

2.3.6. Liquid water sorption

The liquid water sorption measurements were performed by measuring the variation of the mass gain of samples (initially dried) immersed in pure water (MilliQ) until the equilibrium was reached. Four measurements were realised at 25 °C on each film ($A = 4 \text{ cm}^2$) with a balance of mass resolution of 0.1 mg. The transient regime of the sorption kinetic corresponding to the plot "mass gain vs. time" allows calculating the diffusion coefficients D_1 and D_2 . By applying the Fick's laws, the diffusion coefficient D_1 was deduced from the first half-sorption for short times of sorption and the diffusion coefficient D_2 was deduced from the second half-sorption for longer times²⁴.

3 Results and discussion

3.1. Structural characterisation

A detailed analysis of the state of dispersion of nanoclay in P3HB4HB matrix was necessary to correlate the microstructure of nanocomposite films with the transport properties. This study was carried out by WAXD measurements for 2θ angles ranged from 2° to 10°. The WAXD patterns obtained for the C30B, the P3HB4HB matrix and the P3HB4HB/C30B nanocomposites are gathered in Figure 1.

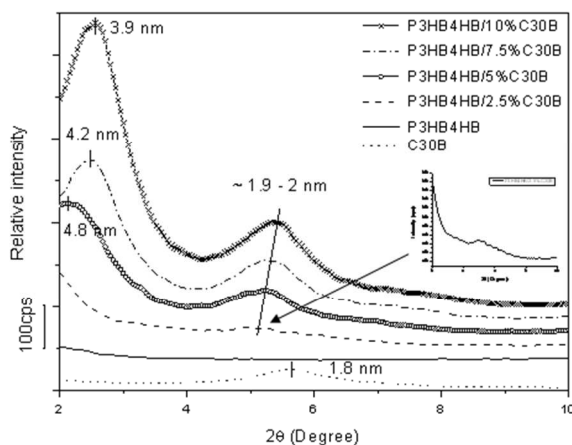


Figure 1: WAXD patterns for the C30B, the P3HB4HB matrix and the P3HB4HB/C30B nanocomposites.

The C30B clay is characterised by a diffraction peak centered on $2\theta = 5.6^\circ$ which is characteristic of the distance between the nanoclay platelets. Taking into account the Bragg law, it is possible to determine the basal spacing d_{001} associated to this peak. The d_{001} value found for the C30B is around 1.8 nm, which is in accordance with the literature and with the values given by the supplier of the clay^{19,25}. As expected, the P3HB4HB matrix pattern does not exhibit diffraction peaks in the selected 2θ angle range. Concerning the nanocomposites, each film shows a diffraction peak in the range of $5^\circ < 2\theta < 5.5^\circ$ generally attributed to the presence of aggregated nanoclays in the materials^{25,26}. It is interesting to note that the more the fraction of C30B increases and the more the intensity

of this peak increases, suggesting that the quantity of aggregates increases with the nanoclay content. This characteristic peak of clay is present on P3HB4HB/2.5%C30B nanocomposite pattern but with a very low intensity because of the low concentration in aggregates in this nanocomposite. It can be observed when modifying the scale of y axis. This peak is shifted to lower 2θ than neat clay value which indicates there should be some interactions anchoring between polymer and nanoclay. However, it is generally assumed that the interactions between the nanoclays and the PHA are mainly hydrogen bonding and not chemical interactions^{19,25,26,27}. Moreover, some authors have shown that the dispersion of nanoclays in PHA polymers is not achieved without the presence of the surfactant due to the lack of compatibility between native clays and PHA^{28,20}. A shift of this diffraction peak to higher 2θ angles is observed when the nanoclay content increases. This evolution can be explained by a concentration effect, because the individualisation of nanoclay platelets is more difficult at high nanoclay content. Another diffraction peak is observed for $2\theta < 4^\circ$. This diffraction peak is characteristic of intercalated structures probably due to the presence of polymer chains between the nanoclay platelets. The basal spacing d_{001} value decreases from 4.8 nm to 3.9 nm when the nanoclay content increases (Table 1). These results confirm that the individualisation is clearly dependent on the C30B fraction. For the P3HB4HB/2.5%C30B nanocomposite, no diffraction peak is observed in the range of $2^\circ < 2\theta < 4^\circ$ suggesting that the nanoclay platelets are rather individualised, such as an exfoliated structure, as observed by Wang *et al.*²⁶ The WAXD pattern of P3HB4HB matrix exhibits characteristic peaks of crystalline region at 2θ angles above 10° (not shown in Figure 1). Similar X-ray patterns were obtained for the P3HB4HB/C30B nanocomposites, whatever the nanoclay loading.

Samples	2θ (degree)	d_{001} (nm)	α_{exp}
C30B	5.6	1.8	100-150 ^a
P3HB4HB	-	-	-
P3HB4HB/2.5%C30B	-	-	37
P3HB4HB/5%C30B	2.1	4.8	38
P3HB4HB/7.5%C30B	2.5	4.2	41
P3HB4HB/10%C30B	2.6	3.9	32

^a reference²⁸

Table 1: 2θ angle, basal spacing d_{001} and experimental aspect ratio α_{exp} of the C30B, the P3HB4HB matrix and the P3HB4HB/C30B nanocomposites.

The TEM images were taken from a representative region of the P3HB4HB/C30B nanocomposites in order to evaluate the dispersion of clay (Figure 2).

All images show the presence of small tactoids (structure composed of a small number of nanoclay platelets) randomly dispersed. The presence of large aggregates ($\sim 1 \mu\text{m}$ long and 500 nm thick) is also observed especially at high nanoclay content as showed for the P3HB4HB/7.5%C30B nanocomposite (Figure 2-f). These observations are in accordance with the WAXD measurements and confirm the presence of a concentration effect. At high magnification, all nanocomposites are characterised by intercalated structures (e.g. P3HB4HB/7.5%C30B nanocomposite given in Figure 2-e) as previously shown on WAXD patterns. The presence of free nanoclay platelets, *i.e.* of exfoliated clays, is also observed (Figure 2 d-e). Concerning P3HB4HB/2.5%C30B, Figure 2-a shows the presence of very small tactoids without real

intercalated structure. In addition to the coexistence of these different structures in the nanocomposites and a dependence with the nanoclay amount, an alignment of the nanoclay platelets is also clearly observed. It is reasonable to assume that the structure of this nanocomposite is close to an exfoliated structure as suggested previously from the WAXD pattern.

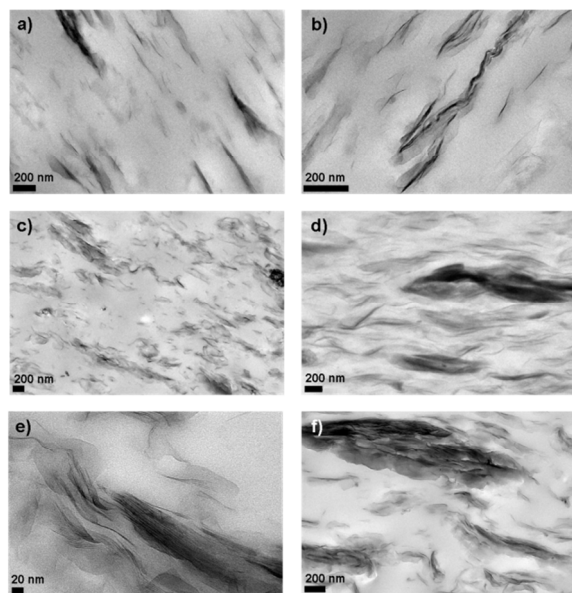


Figure 2: TEM pictures of the P3HB4HB/C30B nanocomposites: a) P3HB4HB/2.5%C30B; b) P3HB4HB/5%C30B; c) e) and f) P3HB4HB/7.5%C30B; d) P3HB4HB/10%C30B.

Some authors^{29,30} have mentioned that the sample preparation processes can promote the orientation of nanoclay platelets. A mean aspect ratio α_{exp} was calculated for each nanocomposite to complete the analysis of the state of dispersion (Table 1). The α_{exp} values vary from 32 to 41 which is largely lower than the theoretical value of montmorillonite nanoclays (α between 100 and 15²⁸). In the literature, the same discrepancy between experimental and theoretical values was also noted and attributed in part to the errors measurements due to the overlapping and the shape of nanoclay platelets^{30,31}.

The thermal behaviour of P3HB4HB/C30B nanocomposites was evaluated by DSC measurements. The values of the glass transition temperature T_g obtained for the matrix and the filled P3HB4HB films are gathered in Table 2.

Samples	T_g (°C)	T_m (°C)	T_c (°C)	X_c (%)
P3HB4HB	-6 ± 1	159 ± 1	107 ± 1	32 ± 3
P3HB4HB/2.5%C30B	-7 ± 1	161 ± 1	106 ± 1	32 ± 3
P3HB4HB/5%C30B	-6 ± 1	159 ± 1	107 ± 1	31 ± 3
P3HB4HB/7.5%C30B	-6 ± 1	159 ± 1	106 ± 1	32 ± 3
P3HB4HB/10%C30B	-5 ± 1	159 ± 1	106 ± 1	34 ± 3

Table 2: Glass transition temperature T_g , melting temperature T_m , crystallisation temperature T_c and crystallinity degree X_c for the P3HB4HB matrix and the P3HB4HB/C30B nanocomposites.

P3HB4HB matrix exhibits a T_g equal to -6 °C. No change of the T_g value is found after incorporation of nanoclay. Similar results have been previously found by on different PHA/nanoclays nanocomposites^{19,26}. In addition, the DSC measurements allow analysing the crystalline phase which

plays a key role in the barrier properties³². The thermogram for P3HB4HB matrix obtained during the heating (Figure 3) exhibits complex endotherms with two large melting zones; the first from 35 °C to 125 °C and the second from 140 °C to 170 °C. Although the melting behaviour is not yet clearly clarified, Wen *et al.*⁹ have suggested the existence of zones more or less enriched in 3HB units. The melting peak in the 140-170 °C range would correspond to the melting of crystals rich in 3HB units, while the broad peak in the 35-125°C range would correspond to the melting of more or less perfect crystals in 4HB units-enriched zones⁹. In presence of nanoclay, no noticeable change (shape and position) of endotherms is observed (Figure 3). This result is confirmed by the constant value of the melting temperature after incorporation of C30B (T_m , temperature determined at the top of the second melting peak, Table 2). Thus, the addition of C30B does not seem to influence the perfection and the size of the P3HB4HB crystallites.

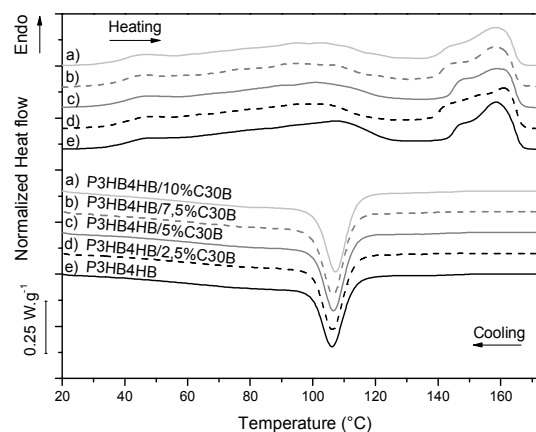


Figure 3: DSC heating and cooling curves for the P3HB4HB matrix and the P3HB4HB/C30B nanocomposites.

Concerning the thermograms obtained during the cooling (Figure 3), each sample presents an exothermic peak characteristic of the crystallisation phenomenon. This peak present no significant variation of shape, position and crystallisation temperature T_c (Table 2) when the C30B fraction increases, suggesting that the nanoclay does not act as a nucleating agent³³ which usually leads to a high shift of T_c ³⁴. These results are in opposition with some available data in the literature where it is generally assumed that C30B may act as a nucleating agent^{19,26} and able to induce defects in the crystalline phase^{19,27}. Such discrepancy in the structural modification induced by nanoclay can be explained by the interactions between filler and the organic matrix but also by the preparation of the nanocomposite films. From the enthalpies determined from endotherms during the heating, the crystallinity degree X_c can be calculated (Table 2). Taking into account the uncertainties, it seems that the nanoclay does not change the crystallinity degree. On the whole, the DSC measurements have shown that the nanoclay has no influence on the crystalline phase. Finally, there is no change in the melting of the P3HB4HB copolymer because the nanoclays are mainly excluded from the crystalline phase and thus are more or less dispersed only in the polymer amorphous phase. There is also no change in crystallisation of the P3HB4HB polymer as C30B does not act as a nucleating agent. These two experimental points were studied and confirmed in a previous paper³³ using DSC, WAXD and Broadband Dielectric

Spectroscopy (BDS). This behavior is probably due to the preparation of the samples.

3.2. Gas transport properties

The study of gas transport properties was carried out with three different molecular probes, nitrogen (N_2), oxygen (O_2) and carbon dioxide (CO_2), which differ by their dynamic diameter³⁵, Van der Waals molar volume³⁶ and their ability to condense³⁵ (critical temperature). The P values obtained for the P3HB4HB matrix and the P3HB4HB/C30B nanocomposites are gathered in Table 3.

Samples	P_{N_2} (Barrer)	P_{O_2} (Barrer)	P_{CO_2} (Barrer)
P3HB4HB	0.074 ± 0.004	0.196 ± 0.005	0.65 ± 0.03
P3HB4HB/2.5%C30B	0.072 ± 0.009	0.151 ± 0.009	0.68 ± 0.02
P3HB4HB/5%C30B	0.063 ± 0.005	0.121 ± 0.006	0.81 ± 0.02
P3HB4HB/7.5%C30B	0.055 ± 0.008	0.111 ± 0.003	0.85 ± 0.03
P3HB4HB/10%C30B	0.047 ± 0.002	0.103 ± 0.002	0.96 ± 0.08

Table 3: Nitrogen, oxygen and carbon dioxide permeability coefficients for the P3HB4HB matrix and the P3HB4HB/C30B nanocomposites.

3.2.1. P3HB4HB matrix

For the P3HB4HB matrix, the N_2 permeability coefficient (P_{N_2}) is estimated to 0.074 Barrer. This value is intermediate to those obtained for PHBV (0.02 Barrer³⁷) and PLA (1.3 Barrer, for a L:D ratio of 96:4³⁸). The difference in P observed for these different matrices is clearly linked to the crystallinity degree (32% for P3HB4HB, 57% for PHBV and 2% for PLA). Indeed, the crystalline phase is generally considered as an impermeable phase, thus the more the crystallinity degree is important, the more the permeability is low³². Concerning the oxygen permeability, the P_{O_2} value is equal to 0.196 Barrer, which is closed to the values previously found by Corre *et al.*⁷ for two P3HB4HB matrices such as $P_{O_2} = 0.16$ and 0.21 Barrer (1.16 and 1.51 $cm^3 \cdot \mu m \cdot m^{-2} \cdot day^{-1} \cdot atm^{-1}$, respectively). The small discrepancy in the P_{O_2} values can be explained by the P3HB4HB copolymer used (4HB unit content, molecular weight), the sample preparation and the experimental methods (moisture content). As for nitrogen, compared to other natural polyesters, P3HB4HB shows a P_{O_2} value intermediate to PHBV (0.26 $cm^3 \cdot \mu m \cdot m^{-2} \cdot day^{-1} \cdot atm^{-1}$ / 0.036 Barrer⁷) and PLA (3.3 Barrer³⁸), that can be easily explained by the difference of crystallinity. P3HB4HB shows a carbon dioxide permeability coefficient P_{CO_2} equal to 0.65 Barrer. Again and as expected, this value is higher than the value of PHBV (0.15 Barrer³⁷) and largely lower than the value of PLA (10.2 Barrer³⁸). It is not surprising that the permeability of the P3HB4HB matrix follows the sequence $P_{N_2} < P_{O_2} < P_{CO_2}$. Similar results were reported by Van Krevelen³⁹ for dense and homogenous matrices. This order was explained by the difference in the dynamic diameters of the diffusing molecules and their ability to condense (critical temperature)⁴⁰. Indeed, N_2 molecule present a higher dynamic diameter than O_2 and CO_2 molecules ($d(N_2) = 3.64 \text{ \AA}$, $d(O_2) = 3.46 \text{ \AA}$, $d(CO_2) = 3.3 \text{ \AA}$), while CO_2 molecule is characterised by a high condensability due to its large critical temperature ($T_{crit}(N_2) = -147 \text{ }^\circ C$, $T_{crit}(O_2) = -118 \text{ }^\circ C$, $T_{crit}(CO_2) = 31 \text{ }^\circ C$)³⁵.

3.2.2. P3HB4HB/C30B nanocomposite films

After incorporation of nanoclays, the P_{N_2} decreases from 0.074 Barrer for the P3HB4HB matrix to 0.047 Barrer for the highest filled nanocomposite, with 10 wt% of C30B (Table 3). The

relative permeability P_R , defined by the ratio of the nanocomposite permeability to the matrix permeability, decreases with the nanoclay content (Figure 4).

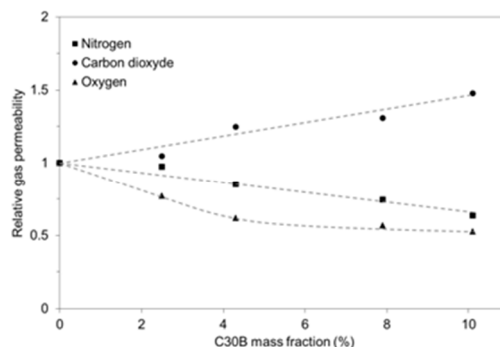


Figure 4: Relative gas permeability of the nanocomposite as a function of the C30B content: nitrogen (■), oxygen (▲), carbon dioxide (●).

This result cannot be attributed to a variation of crystallinity since the crystalline phase is not affected by the presence of nanoclay, as previously shown. In order to determine the origin of the improvement of barrier properties with the nanoclay content, it is necessary to differentiate the effects of the kinetic and thermodynamic contributions on the permeation process. The kinetic aspect of the transfer of molecules through the matrix is characterised by the diffusion coefficient D while the dissolution of molecules in the matrix is characterised by the solubility coefficient S . Since all samples were at a rubbery state at 25 °C (measurement temperature), it is possible to assume that S is the ratio of P to D . The nitrogen diffusion coefficients D_{N_2} and the nitrogen sorption coefficients S_{N_2} for the P3HB4HB matrix and the P3HB4HB/C30B nanocomposites are gathered in Table 4. Concerning D_{N_2} , an increase is observed after incorporation of nanoclay especially for high content. This result is surprising because it is widely-known that the addition of nanoclay induces tortuosity effects in the material leading to increase the diffusion pathway and thus reducing the global diffusivity.

Samples	D_{N_2}	S_{N_2}	D_{O_2}	S_{O_2}	D_{CO_2}	S_{CO_2}
P3HB4HB	6.7 ± 0.2	11.0 ± 0.3	3.1 ± 0.3	64.1 ± 2.0	9.0 ± 0.4	70 ± 6
P3HB4HB/2.5%C30B	8.7 ± 0.6	8.3 ± 1.2	34.9 ± 3.1	4.3 ± 0.1	9.0 ± 0.3	75 ± 3
P3HB4HB/5%C30B	13.9 ± 1.6	4.7 ± 0.8	10.8 ± 0.4	11.2 ± 0.1	8.2 ± 0.4	100 ± 7
P3HB4HB/7.5%C30B	12.2 ± 1.8	4.7 ± 1.8	12.5 ± 2.0	9.1 ± 1.2	8.8 ± 0.2	102 ± 10
P3HB4HB/10%C30B	12.1 ± 0.8	3.9 ± 0.3	11.7 ± 0.8	8.9 ± 0.6	8.3 ± 0.9	116 ± 7

D : 10^9 in $cm^2 \cdot s^{-1}$, S : 10^4 in $cm^3(STP) \cdot cm^{-3} \cdot cmHg^{-1}$

Table 4: Nitrogen, oxygen, carbon dioxide diffusion and solubility coefficients for the P3HB4HB matrix and P3HB4HB nanocomposites.

It is unlikely that nanoclays do not provide tortuosity effects. Therefore it can be considered that antagonism effects occur during the permeation process with a predominant effect that leads to increase the D_{N_2} with the nanoclay content. In this way, we must take into account the presence of interface effects due to a partial compatibility between matrix and C30B. These interfaces with low cohesion would induce an increase of free volume⁴¹ which enhances the nitrogen mobility and counterbalances the tortuosity effect. Moreover, the presence of large aggregates would also lead to increase the free volume⁴¹ and so favours the nitrogen diffusion. For S_{N_2} , a decrease is observed after incorporation of nanoclay. This expected result

is related to the fact that the dissolution of N_2 occurs only in the amorphous phase of the nanocomposite and so decreases with the nanoclay content⁴². To conclude, it is interesting to note that the barrier properties of P3HB4HB/C30B nanocomposites towards nitrogen are mainly governed by the solubility while for the diffusivity the tortuosity effect induced by the filler is offset by interface effect involving free volume which is at the origin of the increase of the nitrogen diffusivity.

Barrier properties of P3HB4HB nanocomposites were also investigated with oxygen as a molecular probe. A large variation in the values of P_{O_2} for the nanocomposites was observed after incorporation of nanoclay: P_{O_2} decreases from 0.196 Barrer for the P3HB4HB matrix to 0.103 Barrer for the highest filled nanocomposite (10 wt% of C30B) (Table 3). This tendency is similar regarding the literature on biopolyester/nanoclay nanocomposites^{29,43,44} for which a decrease of P_{O_2} is generally observed after incorporation of nanoclay. The oxygen diffusion coefficients D_{O_2} and the sorption coefficients S_{O_2} for the P3HB4HB matrix and the P3HB4HB/C30B nanocomposites were determined to interpret these results (Table 4). The D_{O_2} values increase after incorporation of nanoclay even for low content. As previously explained, the presence of nanoclay should induce tortuosity effect in the material leading to reduce the diffusivity. Once again, these results can be explained by the partial compatibility between matrix and C30B and the presence of large aggregates which increase the free volume and so the oxygen mobility. Due to their low size, O_2 molecules would diffuse more easily in the free volume resulting from the low cohesion interfaces between matrix, filler and aggregates. Indeed, although the platelets are aggregated, the space between the layers (interlayer space) is still present. This space (about 0.6 to 0.8 nm) is sufficient for the diffusion of small molecules like O_2 . The more aggregates are, the more this phenomenon is marked. The O_2 solubility in P3HB4HB matrix appeared larger than N_2 solubility. This feature is explained by the highest condensability of O_2 due to its highest critical temperature ($T_{crit}(N_2) = -147\text{ }^\circ\text{C}$, $T_{crit}(O_2) = -118\text{ }^\circ\text{C}$). As for N_2 , S_{O_2} values decreased after incorporation of nanoclay because of the reduction of the total amorphous phase content in which the dissolution of O_2 occurs⁴².

The resulting permeability ($P = D \times S$) is then controlled by the solubility, the permeability of the matrix being higher for O_2 (3 times more) than for N_2 (Table 4). As expected with the barrier effect induced by fillers in the matrix, P_{O_2} and P_{N_2} of nanocomposites are decreased, but if P_{O_2} remains higher than P_{N_2} , the ratio is less than for the unfilled matrix. Therefore, the relative permeability P_R defined by the ratio of the nanocomposite permeability to the matrix permeability appeared lower for O_2 than for N_2 (approximately 2/3 times lower) (Figure 4).

Finally, the permeability measurements were completed by testing carbon dioxide as a diffusing molecule. The permeability coefficients P_{CO_2} for the P3HB4HB/C30B nanocomposites are gathered in Table 3. An unexpected increase of P_{CO_2} is observed with the increase of the nanoclay content (Figure 4). Indeed, this result is surprising because there is usually a decrease of P_{CO_2} with the nanoclay content as previously observed by different authors^{45,46}. A detailed analysis of permeability components, D_{CO_2} and S_{CO_2} (Table 4), is again required to explain this result. For D_{CO_2} , no significant variation is observed which confirms the previous result obtained with nitrogen where the tortuosity effect was counterbalanced by the presence of matrix/filler interfaces of

less cohesion and the high proportion of aggregates. However, the fact that the CO_2 diffusivity remains practically constant whatever the filler content, in opposite to N_2 and O_2 , would mean that some interactions take place at the matrix/nanoclay interface between CO_2 molecules and C30B and thus reducing the mobility of CO_2 molecules. This result is consistent with the solubility data. Indeed, concerning S_{CO_2} , a strong increase is observed with the nanoclay content which is probably due to the high affinity between CO_2 molecules and the quaternary ammonium cations present in C30B surfactant⁴⁷. This affinity would contribute to the facilitated transport phenomena of CO_2 and finally to an increase of P_{CO_2} when the nanoclay content increases. This effect was not observed for N_2 and O_2 because S_{O_2} and S_{N_2} values were ten times lower than S_{CO_2} (Table 4). The relative permeability for CO_2 appeared higher than for O_2 and N_2 as P values depend mainly on the solubility S (Figure 4). D values were almost found to be similar, independently of the three tested gases

3.2.3. Selectivity

In the light of the previous results, it is interesting to calculate the selectivity coefficients α_{O_2/N_2} , α_{CO_2/N_2} , and α_{CO_2/O_2} for the P3HB4HB/C30B nanocomposites (Table 5).

Samples	α_{O_2/N_2}	α_{CO_2/N_2}	α_{CO_2/O_2}
P3HB4HB	2.6	8.8	3.3
P3HB4HB/2.5%C30B	2.1	9.4	4.5
P3HB4HB/5%C30B	1.9	13	6.7
P3HB4HB/7.5%C30B	2.0	15	7.6
P3HB4HB/10%C30B	2.2	20	9.3

Table 5: Selectivity coefficients, and for the P3HB4HB matrix and the P3HB4HB nanocomposites.

The α_{O_2/N_2} values obtained are quite close to that obtained for the matrix, so that the incorporation of nanoclays does not improve the separation between N_2 and O_2 . The barrier effect induced by the presence of nanoclay in P3HB4HB is similar for N_2 and O_2 , keeping in mind that the decrease in solubility is at the origin of this effect. The low O_2/N_2 selectivity would be due to the loss of selectivity of diffusivity because of the large free volume created at the interfaces between matrix and fillers. In contrast, because of the facilitated transport of CO_2 , the selectivity coefficients α_{CO_2/N_2} and α_{CO_2/O_2} increase with the nanoclay content. Thereby, the highest filled nanocomposite, P3HB4HB/10%C30B, appears as a good candidate to eliminate CO_2 from air which is considered as a greenhouse gas. By extrapolation, P3HB4HB based nanocomposites with high C30B content would be promising materials for gas separation in membrane processes.

3.2.4. Modeling using a geometrical approach

In literature, several authors were successful with the simulation of the variations of the relative permeability as a function of the nanoclay content in order to correlate the transport properties to the nanocomposite structure^{30,31}. In this work, the well-known Bharadwaj model¹⁸, based on a geometrical approach derived from the Nielsen model¹⁷, was chosen to fit the variations in the nitrogen permeability. This model takes into account the mass fraction of nanoclay, the aspect ratio of filler α and an orientation factor o which characterise the orientation of the nanoclay in the nanocomposite:

$$P_R = \frac{(1-\phi)}{1 + \frac{\alpha \phi}{3} \times \left(\frac{1}{\phi} + \frac{1}{2} \right)} \quad \text{with} \quad \phi = \left(1 + \frac{\rho_i \cdot (1-\phi_w)}{\rho_p \cdot \phi_w} \right)^{-1} \quad (6)$$

P_R represents the relative permeability, ρ_i is the volumetric mass density of the impermeable phase (C30B, $\rho_i = 1.98 \text{ g.cm}^{-3}$) and ρ_p is the volumetric mass density of the permeable phase (PHBV matrix, $\rho_p = 1.25 \text{ g.cm}^{-3}$). $\phi = 1/2 (3 \cos^2 \theta - 1)$ represents the orientation factor of the nanoplatelets with θ the angle between the plan of nanoclay platelets and the perpendicular to the surface film.

The Bharadwaj model was applied by following two approaches; the first one consists in determining an orientation factor o for each nanocomposite from the values of the mean aspect ratio α_{exp} determined from the TEM images (Table 6), the second consists in determining an aspect ratio α_{calc} from three representative orientation factors o ($o = 0$ for a random orientation, $o = 0.5$ for a semi-oriented orientation and $o = 1$ for an orientation perpendicular to the flux direction) (Table 7).

Samples	α_{exp}	o	RSS
P3HB4HB/2.5%C30B	37	-0.4	0.00005
P3HB4HB/5%C30B	38	-0.1	0.00002
P3HB4HB/7.5%C30B	41	-0.1	0.00001
P3HB4HB/10%C30B	32	0.2	0.00010

Table 6: Orientation factors o for P3HB4HB nanocomposites calculated from the aspect ratio α_{exp} of nanoclay platelets experimentally determined from the TEM pictures.

o	α_{calc}	RSS
0	35	0.0071
0.5	18	0.0071
1	12	0.0071

Table 7: Average aspect ratio α_{calc} calculated from three representative orientations of the C30B nanoclay platelets (through the orientation factor o).

In both cases, the accuracy of the fitting was evaluated through the Residual Sum of Square (RSS). The simulated curves are plotted in Figure 5.

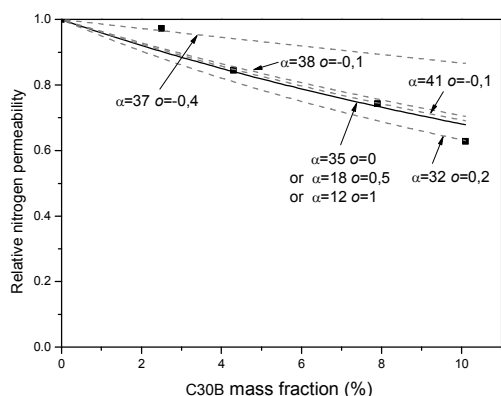


Figure 5: Experimental data (■) and fitting of the relative nitrogen permeability as a function of the C30B content. The gray line (---) and the black line (—) represent respectively the simulations realised with α_{exp} and three representative orientation factor.

For the nanocomposites containing 5, 7.5 and 10 wt% of C30B, the orientation factor o determined with the first approach vary from -0.1 to 0.2 (Table 6). These results suggest that the orientation of nanoclay in nanocomposite is largely random. The values of α_{calc} deduced from the second approach vary from 12 to 35 depending on the imposed o value (Table 7). From these values and by considering the values of α_{exp} , it is reasonable to consider that o is likely close to 0. Thus, both approaches using the Bharadwaj model are consistent with the hypothesis of a largely random orientation of nanoclay. However, these results are in contradiction with the TEM observations where a significant orientation of nanoclay was observed (Figure 2). Thus, an orientation factor o found to be close to 1 would be more appropriate. The discrepancy between the fitting and the TEM observations reflects the limit of Bharadwaj model only based on geometrical aspects and neglecting other relevant factors like the interface effects and the stiffness caused by the presence of fillers and that may influence the diffusion mechanisms. For the P3HB4HB/2.5%C30B nanocomposite, the orientation factor determined with the first approach is equal to -0.4 which corresponds to an orientation of the nanoclay platelets parallel to the diffusion flow. This result is in accordance with the TEM observations where a significant orientation of nanoclay in the matrix was highlighted. However, this orientation is surprising compared to other nanocomposites (orientation factor o close to 1) while all nanocomposites were processed using the same protocol.

3.3. Water transport properties

Water transport properties of P3HB4HB/C30B nanocomposites were evaluated to determine the interactions between water, matrix and C30B. The water permeability coefficient P_{H_2O} for the P3HB4HB matrix and the P3HB4HB/C30B nanocomposites are given in Table 8.

Samples	P_{H_2O} (Barrer)
P3HB4HB	873 ± 31
P3HB4HB/2.5%C30B	945 ± 78
P3HB4HB/5%C30B	753 ± 22
P3HB4HB/7.5%C30B	546 ± 130
P3HB4HB/10%C30B	581 ± 32

Table 8: Water liquid permeability coefficients of the P3HB4HB matrix and the P3HB4HB/C30B nanocomposites.

For P3HB4HB matrix, P_{H_2O} is equal to 873 Barrer. Corre *et al.*⁷ have previously reported permeability coefficients of the same magnitude (between $5.2 \cdot 10^{-12}$ and $5.6 \cdot 10^{-12} \text{ g.m}^{-1}.\text{Pa}^{-1} / 935$ and 1007 Barrer) for two P3HB4HB matrices.

Concerning the P3HB4HB/C30B nanocomposites, a complex behaviour is observed with the increase of the nanoclay content. Indeed, a slight increase of P_{H_2O} is observed for the P3HB4HB/2.5%C30B nanocomposite followed by a decrease for the nanocomposites with higher nanoclay contents. Once again, it is necessary to differentiate the kinetic and thermodynamic contributions of the permeation process to determine the transport mechanisms. To study the kinetic contribution, the water diffusion coefficients cannot be used due to the high uncertainties. For this reason, it is interesting to discuss the values of diffusion coefficients D_1 and D_2 calculated from the liquid water sorption measurements (Table 9).

Samples	$D_1 \cdot 10^{10}$ ($\text{cm}^2 \cdot \text{s}^{-1}$)	$D_2 \cdot 10^{10}$ ($\text{cm}^2 \cdot \text{s}^{-1}$)	Mass gain (%)
P3HB4HB	25.6 ± 0.9	14.1 ± 1.3	2.6 ± 0.1
P3HB4HB/2.5%C30B	23.9 ± 1.4	14.7 ± 1.1	2.8 ± 0.1
P3HB4HB/5%C30B	14.7 ± 1.4	8.4 ± 0.6	3.5 ± 0.1
P3HB4HB/7.5%C30B	11.6 ± 1.4	7.6 ± 2.0	3.9 ± 0.2
P3HB4HB/10%C30B	6.5 ± 0.7	4.6 ± 0.9	4.6 ± 0.3

Table 9: Diffusion coefficients D_1 and D_2 and the mass gain deduced from liquid water sorption kinetics for the P3HB4HB matrix and the P3HB4HB/C30B nanocomposites.

No significant variation of the D_1 and D_2 values is observed between the P3HB4HB/2.5%C30B nanocomposite and the P3HB4HB matrix. This result is explained by the low nanoclay content which cannot induce a sufficient tortuosity effect. For higher nanoclay content, a strong decrease of D_1 and D_2 coefficients is observed and can be clearly attributed to the increase of the diffusion pathway of water molecules due to the tortuosity effect. It can be also suggested that the increase of the stiffness of the macromolecular chains due to the presence of fillers can lead to reduce the mobility of water molecules. In addition, the fact that D_2 coefficient is always lower than D_1 coefficient whatever the nanoclay content would reveal the water cluster formation during the sorption kinetic considering that the mobility of water clusters is more reduced than free water molecules. It can be also noted that the strong interactions between C30B and water molecules can also contribute to trap water molecules at the vicinity of the nanoclay and thus slow down their diffusivity through the film⁴⁸. The thermodynamic contribution can be approached by analysing the variation of the mass gain at equilibrium state deduced from liquid water sorption kinetics (Table 9). An increase of the mass gain is observed with the nanoclay content. This result is explained by the interactions existing between the water molecules and the nanoclay due to the hydrophilic nature of C30B. The water solubility of C30B is higher than that of P3HB4HB polymer, despite the fact that montmorillonite has been organo-modified in order to reduce its water sorption capacity⁴⁹.

Finally, to explain the water behaviour of such nanocomposites with various nanofiller content, it is essential to consider both the kinetic and the thermodynamic contributions of the permeability. For the P3HB4HB/2.5%C30B, the increase of the permeability can be attributed to the water sorption capacity of C30B which prevails on the tortuosity effect. For higher nanoclay contents, the reverse result with an increased permeability is mainly governed by the tortuosity effects in comparison with the interactions between the water molecules and the C30B. However, it is obvious that the transport mechanisms involved in these nanocomposites are more complex so that other factors must be taken into account as previously discussed in the case of the nitrogen permeation. Despite these factors are not clearly identified, it is certainly that the matrix/nanoclay interfaces play a crucial role altering the free volume present in these materials.

4 Conclusions

In this study, P3HB4HB films containing organo-modified montmorillonite C30B were prepared by melt intercalation. The influence of the clay content on morphology, thermal and barrier properties of the films was investigated. WAXD measurements and TEM observations have shown the coexistence of aggregated and intercalated structures with

individual nanoclay platelets and a significant alignment of nanoclay into the nanocomposites. DSC measurements have revealed that the nanoclay does not influence the P3HB4HB crystalline structure because mainly located in the amorphous phase.

The influence of the filler on barrier properties of the P3HB4HB based nanocomposite films was evaluated using various diffusing molecules through gas permeation (CO_2 , N_2 , O_2) and water permeation/sorption measurements. The general trend of the improvement of barrier properties in presence of C30B nanoclay was explained by comparing the kinetic (diffusion) and thermodynamic (sorption) contributions of the permeation process. Therefore, the depth analysis of transport properties of these nanocomposites has highlighted that the barrier effect is really dependent on the penetrant used and cannot be linked only to the tortuosity effect. In this work, it was interesting to show that different aspects can be at the origin of the barrier effect including the key role of the matrix/nanoclay interfaces.

The decrease in N_2 permeability for the nanocomposite was mainly attributed to the decrease of the N_2 solubility inside the P3HB4HB matrix since the tortuosity effect induced by the filler was not enough to reduce the N_2 diffusivity. This result has also revealed the presence of free volume at the matrix/nanoclay interfaces and in the free spaces between the layers of the filler aggregates. The modeling of the experimental permeation data has shown the limits of the conventional Bharadwaj model based only on geometrical aspects neglecting the influence of the matrix/nanoclay interfaces. The influence of the filler was more pronounced for O_2 than for N_2 due to the larger decrease of O_2 solubility.

The increase in CO_2 permeability with the nanofiller content was surprising but explained by both the presence of a poor matrix/nanoclay interfaces and an increase of solubility due to the high affinity between CO_2 molecules and the quaternary ammonium cations of the filler surfactant. This result is very promising because of the high potential of these nanocomposites for gas separation and in particular for the selective transport of CO_2 that could be enhanced with higher content of C30B, knowing that the facilitated transport of CO_2 in membrane processes is known to be increased in presence of amine and water molecules.

Concerning water permeability, another complex behavior was obtained for the P3HB4HB/C30B nanocomposites resulting from concomitant and antagonist effects. For the P3HB4HB/2.5%C30B, the increase of the water permeability was attributed to the increase of water solubility, due to the hydrophilic character of the filler, which prevails on the tortuosity effect (insufficient at 2.5 wt%C30B). For higher nanoclay content, the opposite situation was observed with an improvement of barrier properties by considering the predominant effect of the tortuosity despite the interactions between water molecules and clay.

To conclude, this work highlights the complexity of the mechanisms of the transport of small molecules inside nanocomposite materials, the dispersion state of the filler but also the matrix/organomodified-nanoclay interfaces being ones of the key factors.

5 Acknowledgements

The authors thank the “Réseau CRUNCH” (Normandy Network) for the financial support of the PhD fellowship of R.

Crétois. The authors are thankful to F. Cuvilly (Institute of Materials Research, Rouen, France) for his help on WAXD measurements and Dr. S. Bellayer (ENSCL, Lille, France) for her technical contribution during TEM observations.

6 Notes and references

^a Normandie Université, France

^b Université de Rouen, Laboratoire Polymères Biopolymères Surfaces, Bd. Maurice de Broglie, F-76821 Mont Saint Aignan Cedex, France

^c UMR 6270 & FR 3038, F-76821 Mont Saint Aignan Cedex, France

^d AMME-LECAP EA 4528 International Laboratory, Université et INSA de Rouen, Avenue de l'Université BP 12, 76801 Saint Etienne du Rouvray Cedex France

^e Department of Polymers and Composites Technology & Mechanical Engineering, Ecole des Mines de Douai, F-59508 Douai Cedex, France

^f Université Lille Nord de France, F-59000 Lille, France

^g UMET, CNRS UMR 8207, École Nationale Supérieure de Chimie de Lille, F-59652 Villeneuve d'Ascq, France.

¹ R. W. Lenz and R. H. Marchessault. Bacterial polyesters: biosynthesis, biodegradable plastics and biotechnology. *Biomacromolecules* 2005, **6**, 1.

² I. Chodak, Polyhydroxyalkanoates: origin, properties and applications; Elsevier: London, 2008.

³ K. Sudesh, H. Abe and Y. Doi. Synthesis, structure and properties of polyhydroxyalkanoates: biological polyesters. *Prog. Polym. Sci.* 2000, **25**, 1503.

⁴ J. M. Lagaron and A. Lopez-Rubio. Nanotechnology for bioplastics: opportunities, challenges and strategies. *Trends Food Sci. Technol.* 2011, **22**, 611.

⁵ G.-Q. Chen and Q. Wu. The application of polyhydroxyalkanoates as tissue engineering materials. *Biomaterials* 2005, **26**, 6565.

⁶ P. A. Holmes. Biologically produced (R)-3-hydroxyalkanoate polymers and copolymers; Elsevier: London, U.K. 1988.

⁷ Y.-M. Corre, S. Bruzard, J.-L. Audic and Y. Grohens. Morphology and functional properties of commercial polyhydroxyalkanoates: a comprehensive and comparative study. *Polym. Test.* 2012, **31**, 226.

⁸ R. Shogren. Water vapor permeability of biodegradable polymers. *J. Environ. Polym. Deg.* 1997, **5**, 91.

⁹ X. Wen, X. Lu, Q. Peng, F. Zhu and N. Zheng. Crystallization behaviors and morphology of biodegradable poly(3-hydroxybutyrate-co-4-hydroxybutyrate). *J. Therm. Anal. Calorim.* 2012, **109**, 959.

¹⁰ M. Kunioka and Y. Doi, Thermal degradation of microbial copolyesters: poly(3-hydroxybutyrate-co-3-hydroxyvalerate) and poly(3-hydroxybutyrate-co-4-hydroxybutyrate). *Macromolecules* 1990, **23**, 1933.

¹¹ H.W. Zhao, Y.J. Bian, Y. Li, Q.L. Dong, C.Y. Han, L.S. Dong. Bioresource-based blends of poly(3-hydroxybutyrate-co-4-hydroxybutyrate) and stereocomplex polylactide with improved rheological and mechanical properties and enzymatic hydrolysis. *J. Mater. Chem. A*, 2014, **2**, 8881.

¹² Y.J. Bian, C.Y. Han, L.J. Han; H.J. Lin, H.L. Zhang, J.J. Bian, L.S. Dong. Toughening mechanism behind intriguing stress-strain curves in tensile tests of highly enhanced compatibilization of biodegradable poly(lactic acid)/poly(3-hydroxybutyrate-co-4-hydroxybutyrate) blends. *RSC Adv.* 2014, **79**, 41722.

¹³ C. Cong, S. Zhang, R. Xu, W. Lu and D. Yu. The influence of 4HB content on the properties of poly(3-hydroxybutyrate-co-4-hydroxybutyrate) based on melt molded sheets. *J. Appl. Polym. Sci.* 2008, **109**, 1962.

¹⁴ M. Kunioka, A. Tamaki and Y. Doi. Crystalline and thermal properties of bacterial copolyesters: poly(3-hydroxybutyrate-co-3-hydroxyvalerate) and poly(3-hydroxybutyrate-co-4-hydroxybutyrate). *Macromolecules* 1989, **22**, 694.

¹⁵ C. Thellen, S. Cheney and J. A. Ratto. Melt processing and characterization of polyvinyl alcohol and polyhydroxyalkanoate multilayer films. *J. Appl. Polym. Sci.*, 2013, **127**, 2314.

¹⁶ S. S. Ray and M. Bousmina. Biodegradable polymer and their silicate nanocomposites: in greening the 21st century materials world. *Prog. Mater. Sci.* 2005, **50**, 962.

¹⁷ L. E. Nielsen. Models for their permeability of filled polymer systems. *J. Macromol. Sci.* 1967, **1**, 929.

¹⁸ R. K. Bharadwaj. Modeling the barrier properties of polymer-layered silicate nanocomposites. *Macromolecules* 2001, **34**, 9189.

¹⁹ P. Bordes, E. Pollet, S. Bourbigot and L. Averous. Structure and properties of PHA/clay nano-biocomposites prepared by melt intercalation. *Macromol. Chem. Phys.* 2008, **209**, 1473.

²⁰ A. Botana, M. Mollo, P. Eisenberg and R.M. Torres Sanchez. Effect of modified montmorillonite on biodegradable PHB nanocomposites. *Appl. Clay Sci.* 2010, **47**, 263.

²¹ R. Luo, K. Xu and G.-Q. Chen. Study of miscibility, crystallization, mechanical properties, and thermal stability of blends of poly(3-hydroxybutyrate) and poly(3-hydroxybutyrate-co-4-hydroxybutyrate). *J. Appl. Polym. Sci.* 2007, **107**, 3402.

²² C. Joly, D. Le Cerf, C. Chappey, D. Langevin and G. Muller. Residual solvent effect on the permeation properties of fluorinated polyimide films. *Sep. Purif. Technol.* 1999, **16**, 47.

²³ M. Métayer, M. Labbé, S. Marais, D. Langevin, C. Chappey, F. Dreux, M. Brainville and P. Belliard. Diffusion of water through various polymer films: a new high performance method of characterization. *Polym. Test.* 1999, **18**, 533.

- ²⁴ N. Follain, J.-M. Valleton, L. Lebrun, B. Alexandre, P. Schaetzel, M. Metayer and S. Marais, Simulation of kinetic curves in mass transfer phenomena for a concentration-dependent diffusion coefficient in polymer membranes. *J. Membr. Sci.* 2010, **349**, 195.
- ²⁵ L. N. Carli, J. S. Crespo and R. S. Mauler. PHBV nanocomposites based on organomodified montmorillonite and halloysite: the effect of clay type on the morphology and thermal and mechanical properties. *Composites Part A* 2011, **42**, 1601.
- ²⁶ K. Wang, Y. Wang, R. Zhang, Q. Li and C. Shen. Preparation and characterization of microbial biodegradable poly(3-hydroxybutyrate-co-4-hydroxybutyrate)/organoclay nanocomposites. *Polym. Compos.* 2012, **33**, 838.
- ²⁷ R. Hema, P. N. Ng and A. A. Amirul. Green nanobiocomposite: reinforcement effect of montmorillonite clays on physical and biological advancement of various polyhydroxyalkanoates. *Polym. Bull.* 2013, **70**, 755.
- ²⁸ P. Bordes, E. Pollet and L. Avérous. Nano-biocomposites: biodegradable polyester/nanoclay systems. *Prog. Polym. Sci.* 2009, **34**, 125.
- ²⁹ N. Tenn, N. Follain, J. Soulestin, R. Crétois, S. Bourbigot and S. Marais. Effect of nanoclay hydration on barrier properties of PLA/Montmorillonite based nanocomposites. *J. Phys. Chem. Part C* 2013, **117**, 12117.
- ³⁰ S. Alix, N. Follain, N. Tenn, B. Alexandre, S. Bourbigot, J. Soulestin and S. Marais. Effect of highly exfoliated and oriented organoclays on the barrier properties of polyamide 6 based nanocomposites. *J. Phys. Chem. Part C* 2012, **116**, 4937.
- ³¹ E. Picard, A. Vermogen, J.-F. Gérard and E. Espuche. Barrier properties of nylon 6-montmorillonite nanocomposite membranes prepared by melt blending: Influence of the clay content and dispersion state: consequences on modelling. *J. Membr. Sci.* 2007, **292**, 133.
- ³² Y. Tsujita, Physical chemistry of membranes; Marcel Dekker: New York, U.S.A., 1992.
- ³³ R. Crétois, L. Delbreilh, E. Dargent, N. Follain, L. Lebrun, J.M. Saiter. Dielectric relaxations in polyhydroxyalkanoates/organoclay nanocomposites. *Eur. Polym. J.* 2013, **49**, 3434.
- ³⁴ Y.J. Bian, L.J. Han, C.Y. Han, H.J. Lin, H.L. Zhang, J.J. Bian, L.S. Dong. Intriguing crystallization behavior and rheological properties of radical-based crosslinked biodegradable poly(3-hydroxybutyrate-co-4-hydroxybutyrate). *Cryst. Eng. Comm.* 2014, **16**, 2702.
- ³⁵ C. Bishop. Roll-to-roll vacuum deposition of barrier coatings; John Wiley & Sons: Hoboken, New Jersey, U.S.A., 2010.
- ³⁶ R. W. Baker and J. G. Wijmans. Membrane separation of organic vapors from gas streams; CRC Press: Boca Raton, U.S.A., 1994.
- ³⁷ N. Follain, C. Chappé, E. Dargent, F. Chivrac, R. Crétois and S. Marais. Structure and barrier properties of biodegradable polyhydroxyalkanoate films. *J. Phys. Chem. Part C* 2014, **118**, 6165.
- ³⁸ H. J. Lehermeier, J. R. Dorgan and J. D. Way, Gas permeation properties of poly(lactic acid). *J. Membr. Sci.* 2001, **190**, 243.
- ³⁹ D. W. Van Krevelen. Properties of polymers; Elsevier: Amsterdam, Nederland, 1990.
- ⁴⁰ L. Lebrun, S. Bruzeau, Y. Grohens and D. Langevin. Elaboration and characterization of PDMS-HfNbO₅ nanocomposite membranes. *Eur. Polym. J.* 2006, **42**, 1975.
- ⁴¹ G. Choudalakis and A. D. Gotsis. Free volume and mass transport in polymer nanocomposites. *Curr. Opin. Colloid Interface Sci.* 2012, **17**, 132.
- ⁴² G. Choudalakis and A. D. Gotsis. Permeability of polymer/clay nanocomposites: A review. *Eur. Polym. J.* 2009, **45**, 967.
- ⁴³ M. D. Sanchez-Garcia and J. M. Lagaron. Novel clay-based nanobiocomposites of biopolyesters with synergistic barrier to UV light, gas, and vapour. *J. Appl. Polym. Sci.* 2010, **118**, 188.
- ⁴⁴ P. B. Messersmith and E. P. Giannelis. Synthesis and barrier properties of poly(ϵ -caprolactone)-layered silicate nanocomposites. *J. Polym. Sci. Part A* 1995, **33**, 1047.
- ⁴⁵ H. C. Koh, J. S. Park, M. A. Jeong, H. Y. Hwang, Y. T. Hong, S. Y. Ha and S. Y. Nam. Preparation and gas permeation properties of biodegradable polymer/layered silicate nanocomposite membranes. *Desalination* 2008, **233**, 201.
- ⁴⁶ O. Gain, E. Espuche, E. Pollet, M. Alexandre and P. Dubois. Gas barrier properties of poly(ϵ -caprolactone)/clay nanocomposites: influence of the morphology and polymer/clay interactions. *J. Polym. Sci. Polym. Phys.* 2005, **43**, 205.
- ⁴⁷ M.-J. Kim, Y.-I. Park, K.-H. Youm and K.-H. Lee. Facilitated transport of CO₂ through ethylenediamine-fixed cation-exchange polysaccharide membranes. *J. Membr. Sci.* 2004, **245**, 79.
- ⁴⁸ P. E. Rouse. Diffusion of vapors in films. *J. Am. Chem. Soc.* 1947, **69**, 1068.
- ⁴⁹ B. Alexandre, D. Langevin, P. Médéric, T. Aubry, H. Courdec, Q.T. Nguyen, A. Saiter and S. Marais. Water barrier properties of polyamide 12/montmorillonite nanocomposite membranes: structure and volume fraction effects. *J. Membr. Sci.* 2009, **328**, 186.